Accepted Manuscript

Phase equilibria in the Co-Mn-Ni system

Yang Zhou, Philip Nash, Xingye Dai, Dongnan Li, Alexandre Alves Silva, Gabriel Ribeiro Lopes Cardoso

PII: S0925-8388(18)34208-7

DOI: https://doi.org/10.1016/j.jallcom.2018.11.087

Reference: JALCOM 48313

To appear in: *Journal of Alloys and Compounds*

Received Date: 15 July 2018

Revised Date: 21 October 2018

Accepted Date: 7 November 2018

Please cite this article as: Y. Zhou, P. Nash, X. Dai, D. Li, A.A. Silva, G.R. Lopes Cardoso, Phase equilibria in the Co-Mn-Ni system, *Journal of Alloys and Compounds* (2018), doi: https://doi.org/10.1016/j.jallcom.2018.11.087.

Co-Mn-Ni Alloy System

Isothermal Section

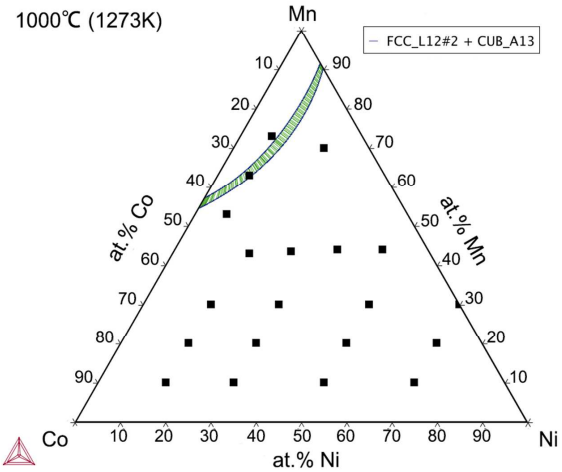

TG&DSC

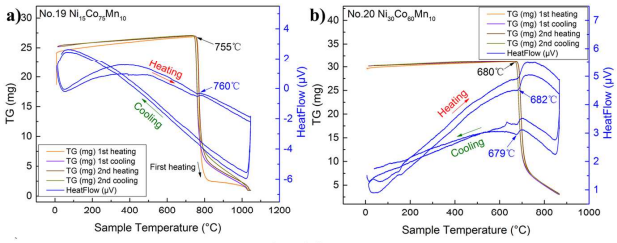

Gleeble Test

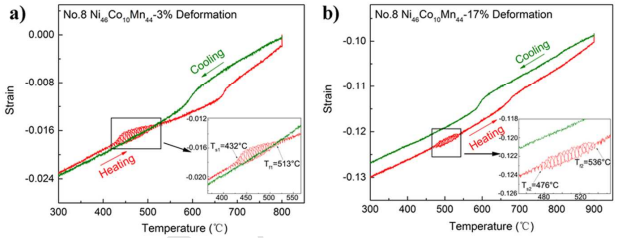

Phase equilibria in the Co-Mn-Ni system

Yang Zhou[*1,2], Philip Nash[*,2], Xingye Dai[2,3] Dongnan Li[2,4], Alexandre Alves Silva[2], Gabriel Ribeiro Lopes Cardoso[2]

ORCID: Yang Zhou: 0000-0002-5543-9366, Philip Nash: 0000-0003-2975-8512

1, Shanghai Key Laboratory of Advanced High-temperature Materials and Precision Forming, Shanghai Jiao Tong University, No. 800, Dongchuan Road, Shanghai 200240, China

2, Thermal Processing Technology Center, Illinois Institute of Technology, Chicago, IL 60616, USA

3, Beijing Institute of Technology, Beijing, 100081, China

4, College of Materials Science and Engineering, Fujian University of Technology, Fuzhou, 350118, China

Abstract

Co-Mn-Ni alloys are promising shape memory alloys and functional materials. However, very limited information can be found regarding the phase transformations and magnetic properties in this ternary system. In this work, a series of 22 Co-Mn-Ni alloys with various compositions were selected and synthesized based on a computed phase diagram. Metallography, X-ray diffraction (XRD), energy dispersive spectroscopy (EDS), differential scanning calorimetry (DSC), hardness and Gleeble tests were used for microstructural characterization and phase transformation investigations. The results indicate that all samples show a face-centered-cubic (FCC) structure after quenching from 1000°C. Phase transformations and Curie temperatures of the samples were obtained through a combined method of analyzing the heat effects and thermogravimetric

* Corresponding author: Yang Zhou, yzhou76@sjtu.edu.cn; Professor Philip Nash, nash@iit.edu

behavior of the alloys in the presence of a magnetic field during differential scanning calorimetry. Thermal expansion tests indicate that the FCC to BCC transformation is a thermoelastic transformation whereas the shape memory effect was not observed in the Co-Mn-Ni alloys tested.

Keywords: high-temperature alloys; phase transitions; X-ray diffraction; magnetic measurements; thermal analysis.

1. Introduction

The Co-Mn-Ni alloy system is the basis for many shape memory alloys such as Co-In-Mn-Ni[1–4], Co-Ga-Mn-Ni[5,6] and Co-Mn-Ni-Sn[7–10] due to the martensitic transformation at specific temperatures. Although some work has been done on these quaternary alloys, there remains a lack of information regarding the Co-Mn-Ni ternary alloy system. Only one liquidus projection[11] and two isothermal sections are reported according to the SpringerMaterials database[12,13], as shown in Fig. 1. The phases and structure data in the ternary system are given in Table 1. The only available experimental isothermal section was established by Köster in 1954[14], which is described as phase equilibria at room temperature (Fig. 1b). The other one is a computed isothermal section at 25°C (Fig. 1c)) based on a coherent potential approximation (CPA) method by Brauwers *et al.* in 1977[15], where they established a model that enables the enthalpy of formation to be computed as a function of the alloy concentration. However these two phase diagrams show completely different phase equilibria at room temperature. Furthermore, it is not convincing to claim that the phase equilibria determined

experimentally correspond to room temperature for high melting alloys due to the extensive time needed to reach equilibrium. As a result, it is necessary for us to revisit this ternary alloy system and determine the phase equilibria experimentally.

The relevant binary phase diagrams (Co-Ni[16], Mn-Ni[16,17] and Co-Mn[14]) have been investigated in previous reports. The phases and structure data in Co-Mn, Co-Ni and Mn-Ni binary systems are shown in Table 1. The published binary systems indicate that the Curie transformation temperature varies with the composition. In the Co-Mn system given by Köster[14], the Curie temperature drops almost linearly from 1121°C (pure Co) to 200°C on addition of 28 at.%Mn. For the Mn-Ni system, an overall phase diagram with Curie temperature was given by Gokcen[16], where the Curie temperature is constant in the two phase regions and some two phase regions can exhibit two Curie temperatures due to the existence of two ferromagnetic phases. The magnetic moment of disordered Mn-Ni alloy in the low content Mn region was investigated by Tange *et al.*[18]. They found that with the increase of Mn content up to 24 at.%, the Curie temperature decreases monotonically and tends to become zero near Ni_3Mn. While in the Co-Ni binary system evaluated by Nash[16], there is complete solid solubility in the face-centered cubic (FCC) γ phase above 422°C. A small region of ω (hcp) phase exists below 422°C because of the polymorphic transformation of Co on cooling from FCC to hexagonal structure. The Curie temperature varies almost linearly in the γ phase from 1121°C for pure Co to 361°C for pure Ni. However, very little information could be found regarding the Curie temperature for Co-Mn-Ni ternary alloys. Köster measured the Curie temperature in this alloy system and plotted Curie temperature isotherms for the Co- and Ni-rich alloys containing up to 30 at.% Mn [14]. There is still a lack of data on

other compositions, which require further investigation.

Shape memory alloys share a property in common that they all undergo a transformation from low temperature martensite to high temperature austenite. The magnetism of the martensite and austenite can be ferromagnetic or paramagnetic or even antiferromagnetic. For thermally induced shape memory effect, the shape memory alloy always has a thermoelastic martensitic transformation. For Mn-Ni(-X) alloys (X=Al, Co, Fe, Ga, In, Sb, Sn *etc.*) and many other shape memory alloys, the transformation from paramagnetic/ferromagnetic martensite to ferromagnetic/paramagnetic austenite has been extensively investigated[19–22]. In the Mn-Ni binary alloy system, Adachi *et al.* found that a martensitic transformation occurs at the near-equiatomic region. The martensite morphology can only be observed when Mn-rich or stoichiometric alloys are quenched from high temperatures within the B2 ordered β phase region where they transform to $L1_0$ ordered θ phase[23].

The martensitic transformation temperatures are not only affected by alloy composition, but also heat treatments like aging. According to Kalvarez *et al.*[24], they found that Fe and Co could significantly increase the Mn-Ni alloy ductility. However, alloy $NiMn_{40}Fe_{10}$ and $NiMn_{40}Co_{10}$ did not undergo a thermoelastic transformation and the martensite structure was FCC, due to the occupation of the third alloy atoms in the Mn and Ni positions, turning the body-centered tetragonal $L1_0$ structure to FCC. Segur *et al.* found that for low cobalt content Ni-Co-Mn-Ga alloy, which undergoes a structural transformation between ferromagnetic austenite and paramagnetic martensite, the aging process shifts the martensite transformation temperature down and raises the magnetic transition temperature.[25]

Due to their unique functional properties, shape memory alloys have been applied in many applications. Ni-Mn-Ga is known as a good candidate for actuator materials because of their high martensitic transformation temperature[19,26]. While due to their low Curie temperatures and low saturation magnetizations, they are less suitable for use in applications as a shape memory alloy. As a result, it becomes essential to find an alloy with both high martensitic transformation temperatures as well as good shape-memory effect. Given all the research into these types of alloys, it is worthwhile determining whether Co-Mn-Ni alloys have a martensitic transformation as well as understanding phase transformation behavior during heat treatment processes.

2. Experiments

In this work, 22 alloy ingots (15~20g) of different compositions were prepared by arc-melting elemental starting materials of Ni shot (99.99% purity), Co pieces (99.99% purity) and Mn pieces (99.95% purity) under argon protection. The ingots were flipped and re-melted 3 times to ensure sufficient mixing and homogeneity, which were then left to solidify on a water-cooled copper plate. The alloy compositions studied in this work were chosen according to the computed isothermal section in Fig. 1c) and are presented in a Gibbs triangle as shown in Fig. 2. The nominal alloy compositions are shown in Table 2. Due to the high vapor pressure of Mn which would cause some mass loss during melting, about 2~3% additional Mn pieces were added to the constituents to obtain the designed alloy compositions.

All samples were homogenized in argon at 1000°C for 24 to 72 h after arc-melting

in order to remove the as-cast structure and reduce the chemical inhomogeneity. Alloys No. 1 through 10 were cold rolled by 30% to help reduce the grain size and further remove chemical segregation on annealing. These samples were then recrystallized at 1000°C for 1h under Ar protection, followed by quenching in water. We also performed a limited investigation on sample $Ni_{50}Co_{10}Mn_{40}$ aged at lower temperature, 800°C for 10min followed by either quenching or slow cooling, respectively.

Optical microscopy was used to investigate the existing phase morphology after each annealing process. Marble's reagent and 0.1N HCl solution were used for etching as one etchant does not work well for all alloy compositions. Back Scattered electron Composition mode imaging (BSC) and Energy Dispersive Spectroscopy (EDS) on a Scanning Electron Microscope (SEM) were used to observe and measure the phase compositions of each sample using an accelerating voltage of 20 kV. The composition result is an average value of 16 to 20 analyses for each phase. Thermo-Calc® with the TCNI8 database was used to calculate the isothermal sections of the Co-Mn-Ni system. X-ray Diffraction (XRD) was performed on a Thermo ARL θ-θ diffractometer using Cu-Kα radiation. For better resolution, the 11-BM high resolution beamline at the Advanced Photon Source (APS) at Argonne National Laboratory was used with high energy X-rays with a wavelength of 0.41422Å. The XRD results were imported and analyzed using the General Structure Analysis System (GSAS) II software package[28].

The thermo-magnetic analysis was performed on a modified Setaram Thermogravimetry (TG) / Differential scanning calorimetry (DSC) SETSYS instrument

with an external electromagnetic field applied. The specimen size was typically 2x2x5mm^3 with a mass of no more than 200mg. A schematic set up and illustration of the DSC apparatus is published elsewhere[29]. The Curie temperature and phase transformation behavior could thus be studied by analyzing the magnetic behavior of Co-Mn-Ni alloys using this combined TG/DSC method. The heating and cooling rate for all experiments was 5°C/min.

For mechanical properties, the hardness of annealed samples was measured using a diamond indenter with a loading of 0.3 kgf for 15s holding time in a Micro-Vickers hardness tester. The hardness values are the average of 7 measurements. In addition, a Gleeble 3500 was used to measure the thermal expansion in order to observe phase transformations during thermal cycles. The sample size was Φ6x28mm^3, and two different heating rates, 1°C/s and 0.033°C/s, were used. A diametrical dilatometer was used which measured the dimension at the position of the control thermocouple.

3. Results and discussion

3.1 Microstructure observation

The microstructural evolution of the alloy samples after different heat treatments is shown in Fig. 3. It can be seen that the cast samples have dendrites and chemical segregation within the grains. According to the liquidus projection in Fig. 1a), all of the samples are located in the Ni, Co rich fcc primary solidification field. As a result, most of the cast samples exhibit similar microstructure. After 1000°C 24h homogenization, the

dendrites were removed and the grains grew to different sizes according to the alloy composition. Then after 30% cold work followed by 1000°C annealing for 1 hour, recrystallization occurred and an obvious grain size reduction was observed in samples No. 2 and 10 (Fig. 3 c) and f)). While in sample No. 21, as shown in Fig. 3 h) and i), it shows no apparent grain size change after annealing at 1000°C for 24h and 72h as expected since it was not cold rolled. In sample No. 2, as shown in Fig. 3c), an abnormal plate-like structure was observed within some grains, which is believed to be a formation of an oxide phase due to high Mn content in this sample. This was later confirmed in EDS analysis.

3.2 Phase equilibria evaluation

Samples No. 1-8 and 11-22 were investigated using BSC observation and EDS analysis, the equilibrium compositions of phases after annealing at 1000°C are listed in Table 3. The EDS results indicate that in high manganese content samples (No. 6, 7 and 8), there is a tendency to pick up oxygen during processing (up to 22 at.% O), forming Mn oxides which make the sample very brittle.

For the alloys investigated, all samples exhibit a single phase after quenching from 1000°C. Combining with the calculated isothermal section from Thermo-Calc® (TCNI8 database), the single phase compositions are superimposed onto the diagram as shown in Fig. 4. It shows that the current experimental results are in a good agreement with the calculated isothermal section. It can be seen that most of the area is FCC single phase,

which is Ni solid solution; the other single phase area is a simple cubic structure, which is Mn solid solution. This indicates that for most of the Co-Mn-Ni alloys investigated in this work except for alloys No. 1 and 3, they are all in an FCC single phase region at 1000 ^{o}C. The optical microstructures confirm the EDS analysis that the alloys are single phase.

3.3 X-ray diffraction results

The X-ray diffraction patterns using Cu-Kα X-rays are summarized and presented in Fig. 5. Most of the samples exhibit a typical face-centered cubic (FCC) crystal structure according to the standard powder diffraction file[30]. However, the location of the diffraction peaks varies as the alloy composition changes, which is due to the difference in atom sizes of each alloy element leading to variations in lattice parameter. The XRD patterns also suggest that preferred orientations (texture) could be found in several samples, such as $Ni_7Co_{30}Mn_{63}$, $Ni_{17}Co_{40}Mn_{43}$ and $Ni_{30}Co_{40}Mn_{30}$ as the XRD samples are bulk instead of powder.

The GSAS II software package[28] was used to determine the lattice parameters of the phases present in each sample. Nevertheless, it can be observed that in sample No. 6 ($Ni_{26}Co_{30}Mn_{44}$), No.7 ($Ni_{36}Co_{20}Mn_{44}$) and No.8 ($Ni_{46}Co_{10}Mn_{44}$), the fluorescence background is strong and the intensities for the characteristic peaks are low and hard to distinguish. Moreover, since peak splitting was observed, which might be due to the existence of a possible second phase that has the same crystal structure and similar lattice parameter, it is hard to distinguish whether the peak split comes from the $K\alpha_2$ peaks or a

second phase.

Therefore, in order to determine the accurate lattice parameters of the FCC phase in each sample, high-energy X-ray diffraction on powder samples was performed at Argonne National Laboratory. The results from the APS beam line experiments are shown in Fig. 6.

The final result shows quite a satisfactory intensity and peak location for each sample. After analyzing with GSAS II, except for sample f (No.3)-$Ni_7Co_{30}Mn_{63}$, all the samples turned out to be single phase FCC structure. It can be seen that for sample $Ni_7Co_{30}Mn_{63}$, some extra peaks appeared, which are located at 11.691°, 11.901°, 12.111°, 18.131° and 19.041°, respectively. These peaks match the pattern of MnO_2, consistent with the microstructure results as mentioned above. Combining both normal and APS X-ray diffraction data, using GSAS II refinement, the lattice parameters could be obtained as shown in Table 4. It shows clearly that the lattice parameter of the FCC phase increases with increasing Mn content due to its larger atomic radius. The result corresponds to the change of the peak location (shifting lower diffraction angles) in lower Mn content samples.

3.4 Hardness test

All the quenched samples were tested using a Micro-Vickers hardness tester. The measured results are shown in Table 5 below. The data from the table indicate that the hardness value generally changes with the content of Mn: the higher the Mn content is,

the higher the hardness of the alloy, ranging from 120 to 190 HV. The hardness result also agrees with the phase equilibrium results discussed above, suggesting that the samples are single phase at 1000°C. Compared with Mn-Ni alloys that have a hardness value of 200~400HV[31], our samples exhibit relatively lower hardness and good ductility, which are easy to roll at room temperature.

We also performed a limited investigation on a sample aged at lower temperature. It shows that, after a nonmagnetic sample $Ni_{50}Co_{10}Mn_{40}$ was aged at 800°C for 10mins followed by slow cooling instead of quenching, not only did the sample become ferromagnetic, but the hardness also increased to twice the value as before. According to S. Hossein Nedjad *et al.*, the precipitation of face centered tetragonal (FCT) θ-NiMn has an age hardening effect in Fe-Ni-Mn alloys[32]. The increased hardness in our samples can be reasonably explained on the basis of such precipitation. XRD analysis was performed and the result showed that after aging at 800°C for 10min and slow cooling, the phase structure transformed from single FCC (a=0.3639nm) to FCC (a=0.3637nm) + FCT (a=0.259579nm, c=0.356905nm, c/a=1.3749, refined in GSAS II), which provides evidence of precipitation of a Mn rich phase.

3.5 Curie temperature

In general, the lattice parameter is expected to affect the Curie temperature, where the Curie temperature decreases with increasing lattice parameter[33]; while with the increasing content of Co, as reported by W. Köster and H. Rittner[14], Curie temperature

increases in the Co-Mn-Ni alloy system. Qualitative measurement with a magnet indicates that most samples are magnetic except for sample No. 1 ($Ni_7Co_{20}Mn_{73}$), No.2 ($Ni_{20}Co_{10}Mn_{70}$) and No.3 ($Ni_7Co_{30}Mn_{63}$). For more accurate characterization, thermogravimetric and DSC analysis in a magnetic field was applied for those samples that show magnetism. The detailed results are shown in Fig. 7 to Fig. 9. The samples underwent two complete heating and cooling cycles.

From the TG vs. Temperature curves in Fig. 7, it shows that the change in apparent mass is quite obvious and the sudden drop of the TG signal indicates that the sample has reached the Curie temperature upon heating, becoming paramagnetic and appearing to *lose* its mass. In this work, the Curie temperature was determined from the turning point where the TG starts to drop on the second cycle. As shown from Fig. 7, for samples with Mn content of 10 at.%, there is a decreasing trend of the Curie temperature (from 755°C to 424°C) with decreasing Co content (from 75 at.% to 20 at.%). Besides, from the TG curves, we could also observe that all samples exhibit a gradual change of mass at the high temperature end instead of a complete sharp change during second heating and cooling process. A possible explanation for this would be due to a second phase precipitation in that temperature range which changes the ferromagnetic phase composition and therefore increased the Curie temperature accordingly. However, further investigation is still needed to verify this assertion. The change in TG curve, on the other hand, indicates that this thermogravimetric method in a magnetic field is a novel method of detecting phase transformations in ferromagnetic samples. Moreover, from the DSC

curves, the Curie transformations could also be detected from the peaks during the heating process, but, compared with the effect on the TG curves, are observable only as small thermal effects.

A similar trend could be observed in Fig. 8, where for samples with Mn content of 20 at.%, the overall Curie temperature decreased compared with those of 10 at.% Mn, ranging from 385°C to 120°C with decreasing Co content. However, for these samples, the Curie transformation effects could not be detected on the DSC curves.

For samples with Mn content up to 30 at.% or even higher, there is no sharp drop of TG on the curves. A gradual mass change was observed instead, as shown in Fig. 9. The small change in TG implies that the Curie point was not detected in the current experimental conditions and is thus assumed to be lower than room temperature. According to Tange *et al.*[34], who investigated the magnetic moment of disordered Ni-Mn alloys in the low Mn content region, with the increase of Mn content up to 24%, the Curie temperature decreases to nearly 0K. It is generally accepted that for Curie temperature measurement, the Curie-Weiss law is followed in the paramagnetic region above the Curie point[35]:

$$\chi=\frac{C}{T-Tc}$$

Where χ is the magnetic susceptibility, C is the Curie constant, T is temperature in Kelvin and Tc is Curie temperature in Kelvin. For the Curie-Weiss law, if the Curie temperature is lower than room temperature, when we heat up a sample from room temperature, we would not see a sudden drop of susceptibility, i.e. a TG drop, upon

heating. Therefore, a gradual mass change is observed instead which reflects only part of the susceptibility curve.

In order to verify this assumption, we placed the sample $Ni_{50}Co_{10}Mn_{40}$ into liquid nitrogen (around 77K) and tested the magnetism with a permanent magnet. The result showed that the paramagnetic sample (at room temperature) became ferromagnetic when held in the liquid nitrogen for 5 minutes.

Fig. 9 d) shows the typical change of sample TG without an applied magnetic field; the sample mass did not change back to the original value due to a small amount of oxidation during the thermal cycling. The mass change is observed to be less than 1 mg, which is very small compared with the effect due to the Curie transformation in applied magnetic field.

3.6 Phase transformation

For Mn-Ni-X alloys (X=Mo, Fe, Ti, Al, Cu, etc) and many other shape memory alloys, the transformation from ferromagnetic/paramagnetic Austenite to paramagnetic/ferromagnetic Martentsite has been investigated for decades. As a diffusionless transformation, it is usually defined by an Austenitic transformation start temperature (A_s) and finish temperature (A_f) as well as a Martensitic transformation start temperature (M_s) and finish temperature (M_f). Moreover, hysteresis was always found between A_p (transformation peak temperature between A_s and A_f) and M_p (peak temperature between M_s and M_f)[20,36].

3.6.1 DSC analysis

Since a martensitic transformation for Co-Mn-Ni alloys is likely to occur in Ni-Mn rich samples, sample No.7 ($Ni_{36}Co_{20}Mn_{44}$), No.8 ($Ni_{46}Co_{10}Mn_{44}$) and No. 9 ($Ni_{50}Co_{10}Mn_{40}$) were examined in the DSC without applied magnetic field. The results are shown in Fig. 10.

From Fig. 10 we can see that all three of these samples show a reversible transformation. Significant endothermic and exothermic peaks could be observed during heating and cooling processes, which denote the Austenitic and Martensitic transformation respectively. The transformation start and finish temperatures (A_s, M_s and A_f, M_f) were determined from the intersections of the tangents of the peak with the extrapolated baseline; the transformation peak temperatures were also evaluated. The results are shown in Table 6. For sample No. 7 and 8, the transformation temperatures are very close to each other as they both have a Mn content of 44 at.%; while for sample No. 9, with a lower Mn content of 40 at.%, the transformation temperature range was shifted to the higher end. This suggests that the Mn content has a major influence on the Austenite and Martensite transformation temperatures.

For the Mn-Ni system mentioned above, a transformation from simple cubic (B2) phase to FCT ($L1_0$) phase occurs near the Mn-Ni equiatomic region. However, Alvarez *et al.*[24] have shown that for $Ni_{50}Mn_{40-x}Fe_x$ alloy, when x is over 7, the FCT ($L1_0$) phase becomes an FCC structure. Due to the similar properties of Co and Fe and their adjacent

position in the periodic table, we may assume that the expected martensitic transformation is a possible FCC to BCC phase transformation in Co-Mn-Ni alloys.

In addition, all of the alloys exhibit an irreversible exothermic peak on the DSC curve before the BCC-FCC transformation during the first heating. One possible explanation of the irreversible peak is that it is the ordering of some disordered domains present after quenching. For a Mn-Ni alloy quenched from 950°C, Adachi and Wayman found that at room temperature it had an ordered FCT structure with c/a=0.95[23], whereas when Mn is substituted by third elements like Fe and Co, the crystal symmetry of the FCT lattice will change and the c/a ratio will rise to 1, which makes the phase structure become disordered FCC. In that case, by quenching, the ordering may not be as complete as in the case of slow cooling. Significant difference in morphology between quenching and slow cooling was also found by Adachi and Wayman. Instead of producing typical martensite upon quenching, find-grained morphologies with {111} twins formed during slow cooling, which was considered to be a “tempered” state due to the internal defects and effective tempering temperatures. These may explain why the exothermic peak does not appear during the second run of each experiment at a slow cooling rate of 5°C/minute.

To determine the effect of cold rolling on the transformation temperature of the sample $Ni_{50}Co_{10}Mn_{40}$, the original sample without cold rolling was also tested with DSC. The results showed that the transformation temperatures shifted no more than 2°C, so we can deduce that the reduced grain size does not affect the transformation temperatures.

Additional samples with higher Co contents were then run in the DSC, and different results were obtained from the previously discussed samples. No obvious peaks were detected from the DSC curves during heating and cooling. This means that with the increasing Co content, the Martentsite/Austenite transformation does not occur.

3.6.2 Thermal expansion test

Thermal expansion tests were also performed on $Ni_{46}Co_{10}Mn_{44}$ samples with a size of Φ6x28mm^3 using a Gleeble 3500 in order to further investigate if the martensitic transformation is a thermoelastic type transformation. The results are shown in Fig.11.

Two different heating rates were used on the sample. From Fig. 11, we can see there is a significant change in diameter during the heating process, suggesting an Austenitic transformation; while during cooling, a less obvious change in diameter was found and it is difficult to determine the Martensitic transformation from the cooling curves. Furthermore, the temperatures of the effects obtained in the dilatometry experiment are different from those obtained from the DSC curves, which is due to a higher heating rate being used in the Gleeble. For thermoelastic transformation, the transformation strain change should be reversible δ type anomalies in martensitic transformations as suggested by Pushin V G [37]. However, from the results in Fig. 11 we can observe an abnormal behavior of the dilatometry: on heating the material rapidly expands and then suddenly drops back close to the original curve. The radial thermal expansion coefficient (CTE) can be determined by linear fitting of the expansion/contraction curve and dividing the

slope by the sample diameter, giving $1.7x10^{-6}$ K^{-1} for the 1°C/s heating curve and $3.3x10^{-6}$ K^{-1} for the 0.033°C/s heating curve. It can be seen that the dilation on the second run is much higher than the first one, which implies a possible precipitation of a second phase (FCT phase) during slow heating, similar to the "tempering" effect as discussed above. In addition, no obvious reversible peaks can be seen; hence no thermoelastic transformation was detected in our thermal expansion tests.

Therefore, a thermal compression test was performed on sample No.8, as shown in Fig. 12. From the strain vs. temperature graph, we can observe an obvious δ type anomaly, which indicates that there could be a thermoelastic transformation. Given that $Ni_{46}Co_{10}Mn_{44}$ already has two basic properties of shape memory alloys, its shape memory effect was also tested in the Gleeble. The sample was deformed 3% and unloaded, after elastic recovery at room temperature it was heated to 800°C at a heating rate of 1°C/s, as shown in Fig. 12 a). The strain value was zero at room temperature prior to application of the compressive stress. No significant recovery of strain in addition to thermal expansion can be observed, so the shape memory effect was hard to distinguish in this case. Therefore, 14% more deformation was applied on the same sample, which was then heated to 900°C with the same heating rate. With larger deformation, significant thermal expansion could be distinguished in Fig. 12 b). However, after heating and cooling, the deformation strain was not recovered since the strain was unchanged, which means the shape memory effect did not occur in this sample. Moreover, strange behavior is observed on the heating curves in both cases. It seems to be a combined strain and

temperature effect since temperature does not continually increase during this process, and this may be due to a deformation twinning phenomenon.

3.7 Phase diagram evaluation

The present work provides us with some first-hand experimental data on the Co-Mn-Ni ternary alloy system. The experimental results indicate that neither of the existing phase diagrams is reliable. The isothermal section of Co-Mn-Ni supposedly corresponding to room temperature determined by Köster does not provide the heat treatment details, leading to uncertainty as to exactly what the results represent. Whether the samples were quenched or slowly cooled to room temperature is unknown. Therefore, the isothermal section in Fig. 1b) is not convincing. More work is needed in order to establish convincing phase equilibria in the Co-Mn-Ni system to produce isothermal sections at additional temperatures from the one determined in this work.

We can use the CALPHAD method to obtain calculated isothermal sections of Co-Mn-Ni alloys at different temperatures. As shown in Fig. 13, Thermo-Calc® software with the TCNI8 database was used for calculations of Co-Mn-Ni isothermal sections.

From the computed phase diagram we can see that the results are very different from the experimental results especially at room temperature, however, we can still see an overall change from multiple phases at low temperature to a large single phase region at high temperature. In addition, a Nishizawa horn, where γ FCC phase separates into ferromagnetic and paramagnetic phases appears between 500°C and 800°C in the

computed phase diagram, but without further experimental investigation we cannot confirm its existence. Experiments to establish this could be performed in a DSC with an imposed magnetic field to measure Curie temperature [29].

4. Concluding remarks

Since the available phase diagrams for the Co-Mn-Ni system are not reliable, the phase equilibria, Curie temperatures and phase transformations in the Co-Mn-Ni alloy system were investigated. The following conclusions can be made:

(1) A partial isothermal section of the Co-Mn-Ni system at 1000°C was established in this work. For the alloys investigated, all samples exhibit a single phase after quenching from 1000°C. The current experimental results are in good agreement with the corresponding calculated isothermal section using Thermo-Calc® (TCNI8 database).

(2) The Curie temperatures were determined using a combined magnetic TG and DSC method for Co-Mn-Ni samples with Mn content of no more than 30 at.%. The Curie temperature of other samples appears to be below room temperature, which is out of measurement range for our experimental apparatus.

(3) The Austenitic and Martensitic transformation temperatures were determined from DSC curves. The results show that the Mn content has a major influence on the Austenitic and Martensitic transformation temperatures. The thermal expansion tests indicated that the FCC-BCC phase transformation is a thermoelastic transformation whereas the shape memory effect was not observed in the Co-Mn-Ni alloys.

(4) In the thermodynamically computed phase diagrams, a Nishizawa horn where γ FCC phase separates into ferromagnetic and paramagnetic phases appears between 500°C and 800°C. Further investigation is needed to verify its existence.

Acknowledgements

This work was performed under National Science Foundation grant DMR 1607943. One of the authors, Yang Zhou is grateful for the financial support from the Chinese Scholarship Council.

Reference

[1] Z. Li, J. Wang, Y. Zhang, K. He, X. Zhao, L. Zuo, G. Hofer, C. Esling, Texturation of Ni-Co-Mn-In Ribbons by Melt Spinning, Adv. Eng. Mater. 12 (2010) 1024–1028.

[2] Takuo Sakon and Shingo Yamazaki and Yasushi Kodama and Mitsuhiro Motokawa and Takeshi Kanomata and Katsunari Oikawa and Ryosuke Kainuma and Kiyohito Ishida, Magnetic Field-Induced Strain of Ni–Co–Mn–In Alloy in Pulsed Magnetic Field, Jpn. J. Appl. Phys. 46 (2007) 995.

[3] J.A. Monroe, I. Karaman, B. Basaran, W. Ito, R.Y. Umetsu, R. Kainuma, K. Koyama, Y.I. Chumlyakov, Direct measurement of large reversible magnetic-field-induced strain in Ni–Co–Mn–In metamagnetic shape memory alloys, Acta Mater. 60 (2012) 6883–6891. doi:10.1016/j.actamat.2012.07.040.

[4] A N Vasiliev and O Heczko and O S Volkova and T N Vasilchikova and T N Voloshok and K V Klimov and W Ito and R Kainuma and K Ishida and K Oikawa

and S Fähler, On the electronic origin of the inverse magnetocaloric effect in Ni–Co–Mn–In Heusler alloys, J. Phys. Appl. Phys. 43 (2010) 055004.

[5] B. Emre, S. Yüce, E. Stern-Taulats, A. Planes, S. Fabbrici, F. Albertini, L. Mañosa, Large reversible entropy change at the inverse magnetocaloric effect in Ni-Co-Mn-Ga-In magnetic shape memory alloys, J. Appl. Phys. 113 (2013) 213905. doi:10.1063/1.4808340.

[6] Y. Wang, C. Huang, J. Gao, S. Yang, X. Ding, X. Song, X. Ren, Evidence for ferromagnetic strain glass in Ni-Co-Mn-Ga Heusler alloy system, Appl. Phys. Lett. 101 (2012) 101913. doi:10.1063/1.4751250.

[7] X. Chen, V.B. Naik, R. Mahendiran, R.V. Ramanujan, Optimization of Ni–Co–Mn–Sn Heusler alloy composition for near room temperature magnetic cooling, J. Alloys Compd. 618 (2015) 187–191. doi:10.1016/j.jallcom.2014.08.032.

[8] D. Cong, S. Roth, L. Schultz, Magnetic properties and structural transformations in Ni–Co–Mn–Sn multifunctional alloys, Acta Mater. 60 (2012) 5335–5351.

[9] D. Cong, S. Roth, M. Pötschke, C. Hürrich, L. Schultz, Phase diagram and composition optimization for magnetic shape memory effect in Ni–Co–Mn–Sn alloys, Appl. Phys. Lett. 97 (2010) 021908.

[10] Zhida Han and Dunhui Wang and Bin Qian and Jinfu Feng and Xuefan Jiang and Youwei Du, Phase Transitions, Magnetocaloric Effect and Magnetoresistance in Ni–Co–Mn–Sn Ferromagnetic Shape Memory Alloy, Jpn. J. Appl. Phys. 49 (2010) 010211.

[11] P. Villars, H. Okamoto, Co-Mn-Ni Liquidus Projection of Ternary Phase Diagram: Datasheet from “PAULING FILE Multinaries Edition – 2012” in SpringerMaterials

(http://materials.springer.com/isp/phase-diagram/docs/c_0200726), Springer-Verlag Berlin Heidelberg & Material Phases Data System (MPDS), Switzerland & National Institute for Materials Science (NIMS), Japan, n.d. http://materials.springer.com/isp/phase-diagram/docs/c_0200726.

[12] P. Villars, H. Okamoto, Co-Mn-Ni Isothermal Section of Ternary Phase Diagram: Datasheet from "PAULING FILE Multinaries Edition – 2012" in SpringerMaterials (http://materials.springer.com/isp/phase-diagram/docs/c_2000200), Springer-Verlag Berlin Heidelberg & Material Phases Data System (MPDS), Switzerland & National Institute for Materials Science (NIMS), Japan, n.d. http://materials.springer.com/isp/phase-diagram/docs/c_2000200.

[13] P. Villars, H. Okamoto, Co-Mn-Ni Isothermal Section of Ternary Phase Diagram: Datasheet from "PAULING FILE Multinaries Edition – 2012" in SpringerMaterials (http://materials.springer.com/isp/phase-diagram/docs/c_0925250), Springer-Verlag Berlin Heidelberg & Material Phases Data System (MPDS), Switzerland & National Institute for Materials Science (NIMS), Japan, n.d. http://materials.springer.com/isp/phase-diagram/docs/c_0925250.

[14] W. Koster, H. Rittner, Synthesis and Characterisation of Co-Mn-Ni Alloys, Z. Metallkde. 45 (1954) 639–642.

[15] M. Brauwers, F. Brouers, On the occurrence of the sigma phase in transition metal alloys, Philos. Mag. 35 (1977) 1105–1109. doi:10.1080/14786437708232649.

[16] P. Nash, Phase Diagrams of Binary Nickel Alloys, 1991.

[17] L. Ding, P.F. Ladwig, X. Yan, Y.A. Chang, Thermodynamic stability and diffusivity of near-equiatomic Ni–Mn alloys, Appl. Phys. Lett. 80 (2002) 1186–1188.

doi:10.1063/1.1450042.

[18] H. Tange, T. Tokunaga, M. Goto, Magnetic Moment and Curie Point of Disordered Ni-Mn Alloys, J. Phys. Soc. Jpn. 45 (1978) 105–109.

[19] A. Drdzeń, T. Goryczka, K. Prusik, H. Morawiec, J. Lelątko, Studies of Plastically Deformed Ni-Mn-Ga Ferromagnetic Shape Memory Alloy, Solid State Phenom. 163 (2010) 123–126.

[20] X. Moya, L. Mañosa, A. Planes, T. Krenke, M. Acet, E.F. Wassermann, Martensitic transition and magnetic properties in Ni–Mn–X alloys, Mater. Sci. Eng. A. s 438–440 (2006) 911–915.

[21] Y. Nakamura, N. Miyata, Exchange Anisotropy of Fe_(Ni_Mn_x)_ Alloys, J. Phys. Soc. Jpn. 23 (1967) 223–229.

[22] T. Bachaga, R. Daly, J.J. Suñol, J. Saurina, L. Escoda, L.G. Legarreta, B. Hernando, M. Khitouni, Effects of Co Additions on the Martensitic Transformation and Magnetic Properties of Ni–Mn–Sn Shape Memory Alloys, J. Supercond. Nov. Magn. 28 (2015) 3087–3092. doi:10.1007/s10948-015-3100-z.

[23] K. Adachi, C.M. Wayman, Transformation behavior of nearly stoichiometric Ni-Mn alloys, Metall. Trans. A. 16 (1985) 1567–1579.

[24] K. Alvarez, H.Y. Kim, S. Miyazaki, Effect of Alloying Elements on Microstructure,Martensitic Transformation and Mechanical Properties of Ni-Mn Based Alloys, J. Mater. Sci. Technol. 25 (2009) 649–654.

[25] C. Seguí, E. Cesari, Ageing effects on structural and magnetic transformations in a Ni–Co–Mn–Ga alloy, Phys. Procedia. 10 (2010) 99–104.

[26] B. Krevet, M. Kohl, D. Brugger, Coupled simulation of the

thermo-magneto-mechanical properties of a Ni-Mn-Ga actuator, Int. J. Appl. Electromagn. Mech. 23 (2006) 125–131.

[27] K.P. Gupta, The Co-Mn-Ni (Cobalt-Manganese-Nickel) system, J. Phase Equilibria. 20 (1999) 527.

[28] B.H. Toby, R.B. Von Dreele, GSAS-II: the genesis of a modern open-source all purpose crystallography software package, J. Appl. Crystallogr. 46 (2013) 544–549.

[29] J. Hasier, M.A. Riolo, P. Nash, Curie temperature determination via thermogravimetric and continuous wavelet transformation analysis, EPJ Tech. Instrum. 4 (2017). doi:10.1140/epjti/s40485-017-0040-y.

[30] Y. Zhou, P. Nash, S.M. Bessa, G.T. Ferrigatto, B.S.V.P. Madureira, A.S. Magalhães, A. Oliveira, G.C. Pereira, L.G. Ribeiro, L.P. dos Santos, A.A. da Silva, J.D. Silva, A.G. Silva, J.M. de Souza, Y.S. Torres, R.L. da Silva, B.F.R.F. de Cunha, Phase Equilibria in the Al-Co-Ni Alloy System, J. Phase Equilibria Diffus. 38 (2017) 630–645.

[31] N. Yang, T. Headley, J. Kelly, J. Hruby, Metallurgy of high strength Ni–Mn microsystems fabricated by electrodeposition, Scr. Mater. 51 (2004) 761–766.

[32] S. Hossein Nedjad, M. Nili Ahmadabadi, T. Furuhara, T. Maki, High resolution transmission electron microscopy study on the nano‐scale twinning of θ‐NiMn precipitates in an Fe–Ni–Mn maraging alloy, Phys. Status Solidi A. 203 (2006) 2229–2235.

[33] S. Greenwald, Changes in Lattice Constant of Cr2O3 near the Curie Temperature, Nature. 177 (1956) 286.

[34] H. Tange, T. Tokunaga, M. Goto, Magnetic moment and Curie point of disordered

Ni–Mn alloys, J. Phys. Soc. Jpn. 45 (1978) 105–109.

[35] Y. Takahashi, On the origin of the Curie-Weiss law of the magnetic susceptibility in itinerant electron ferromagnetism, J. Phys. Soc. Jpn. 55 (1986) 3553–3573.

[36] H.J. Kang, S.K. Wu, L.M. Wu, Martensitic transformation of Ni64Al34Re2 shape memory alloy, Intermetallics. 18 (2010) 123–128.

[37] V. Pushin, A. Korolev, N. Kourov, N. Kuranova, E. Marchenkova, A. Popov, On the effect of cobalt doping on thermoelastic martensitic transformations in ferromagnetic Heusler Ni 50− x Co x Mn 29 Ga 21 magnetically controlled shape memory alloys, Tech. Phys. Lett. 39 (2013) 737–740.

Figure captions

Figure 1. a) Estimated liquidus projection of the Co-Mn-Ni system[27]; b) Experimental isothermal section of Co-Mn-Ni at room temperature[14]; c) Computed isothermal section of Co-Mn-Ni at room temperature[15] (Note that the diagram violates Schreinemaker's rule at the γ phase corner of the 3-phase triangle).

Figure 2. The nominal atomic percent compositions of the Co-Mn-Ni alloys studied in this work.

Figure 3. Optical microstructures of typical Co-Mn-Ni alloys: Alloy 2 $Ni_{20}Co_{10}Mn_{70}$: a) as-cast structure; b) homogenized at 1000°C for 24h; c) cold rolled by 30% followed by 1000°C annealing for 1h; Alloy 10 $Ni_{33}Co_{33}Mn_{34}$: d) as-cast structure; e) homogenized at 1000°C for 24h; f) cold rolled by 30% followed by 1000°C annealing for 1h; Alloy 21 $Ni_{50}Co_{40}Mn_{10}$: g) as-cast structure; h) homogenized at 1000°C for 24h; i) homogenized at 1000°C for 72h.

Figure 4. Isothermal section at 1000°C superimposed on the calculated diagram using Thermo-Calc® (TCNI8 database).

Figure 5. XRD patterns of Co-Mn-Ni alloys after annealing at 1000°C for 24h.

Figure 6. XRD patterns from APS beam line for Co-Mn-Ni alloys annealed at 1000°C: No.2-$Ni_{20}Co_{10}Mn_{70}$, No.3-$Ni_{7}Co_{30}Mn_{63}$, No.4-$Ni_{7}Co_{40}Mn_{53}$, No.5-$Ni_{17}Co_{40}Mn_{43}$, No.6-$Ni_{26}Co_{30}Mn_{44}$, No.7-$Ni_{36}Co_{20}Mn_{44}$, No.8-$Ni_{46}Co_{10}Mn_{44}$.

Figure 7. The TG-DSC vs. Temperature curves of sample a) No.19; b) No.20; c) No.21 and d) No.22 in a magnetic field.

Figure 8. The TG-DSC vs. Temperature curves of sample a) No.15; b) No.16; c) No.17;

and d) No.18 in a magnetic field.

Figure 9. The TG-DSC vs. Temperature curves of sample a) No.14, b) No.12, c) No.5 in a magnetic field and d) TG vs. Temperature curve of sample No. 6 without magnetic field.

Figure 10. Heat flow curves of Co-Mn-Ni alloys: a) No.7 $Ni_{36}Co_{20}Mn_{44}$; b) No.8 $Ni_{46}Co_{10}Mn_{44}$; c) No.9 $Ni_{50}Co_{10}Mn_{40}$.

Figure 11. Thermal expansion test: Temperature vs Dilation curves of $Ni_{46}Co_{10}Mn_{44}$ at different heating and cooling rates. a) First run at 1°C/s; b) Second run at 0.033°C/s.

Figure 12. Temperature vs strain curve of No.8 $Ni_{46}Co_{10}Mn_{44}$: a) first run after 3% deformation; b) second run after 17% deformation.

Figure 13. Computed isothermal sections for Co-Mn-Ni system at different temperatures: a) 25°C; b) 500°C; c) 600°C; d) 800°C using Thermo-Calc®.

Tables

Table 1. Phases and structure data in Co-Mn-Ni system

Phase Label	Published Phase Label	Pearson symbol	Space group
(Mn)rt	α-Mn, β	cI58	I-43m
(Mn)ht1	β-Mn, σ	cP20	$P4_132$
(Mn ht3,Co ht,Ni)	γ, α, γ,Co,γMn,Ni	cF4	Fm-3m
(Mn) ht4	δMn	cI2	Im-3m
γ	(Mn,Ni) (Co,Ni)	cF4	Fm-3m
ω	(Co)rt	hP2	$P6_3/mmc$
B2	MnNi ht2	cP2	Pm-3m
$L1_0$	MnNi ht1	tp4	P4/mmm

Table 2. Nominal composition and amount of cold work in Co-Mn-Ni samples

	Alloy nominal composition	Nominal Composition at.%			Amount of cold work (%)
		Ni	Co	Mn	
1	Ni7Co20Mn73	7	20	73	30
2	Ni20Co10Mn70	20	10	70	30
3	Ni7Co30Mn63	7	30	63	30
4	Ni7Co40Mn53	7	40	53	30
5	Ni17Co40Mn43	17	40	43	30
6	Ni26Co30Mn44	26	30	44	30
7	Ni36Co20Mn44	36	20	44	30
8	Ni46Co10Mn44	46	10	44	30
9	Ni50Co10Mn40	50	10	40	30
10	Ni33Co33Mn34	33	33	34	30
11	Ni15Co55Mn30	15	55	30	0
12	Ni30Co40Mn30	30	40	30	0
13	Ni50Co20Mn30	50	20	30	0
14	Ni70Mn30	70	0	30	0
15	Ni15Co65Mn20	15	65	20	0
16	Ni30Co50Mn20	30	50	20	0
17	Ni50Co30Mn20	50	30	20	0
18	Ni70Co10Mn20	70	10	20	0
19	Ni15Co75Mn10	15	75	10	0
20	Ni30Co60Mn10	30	60	10	0
21	Ni50Co40Mn10	50	40	10	0
22	Ni70Co20Mn10	70	20	10	0

Table 3. Alloy compositions for Co-Mn-Ni alloys annealed at 1000 °C determined using EDS

Alloy No.	Nominal composition	EDS results at.%			Alloy No.	Nominal composition	EDS results at.%		
		Ni	Co	Mn			Ni	Co	Mn
1	Ni7Co20Mn73	7.7	22.8	69.5	13	Ni50Co20Mn30	49.9	20.2	29.9
2	Ni20Co10Mn70	20.7	10.1	69.2	14	Ni70Co00Mn30	69.5	0	30.5
3	Ni7Co30Mn63	5.1	29.4	65.5	15	Ni15Co65Mn20	14.9	64.7	20.4
4	Ni7Co40Mn53	7.1	39.5	53.4	16	Ni30Co50Mn20	29.9	49.9	20.2
5	Ni17Co40Mn43	16.3	39.6	44.1	17	Ni50Co30Mn20	49.9	29.9	20.2
6	Ni26Co30Mn44	25.4	29.2	45.4	18	Ni70Co10Mn20	69.5	10.1	20.4
7	Ni36Co20Mn44	35.9	18.3	45.8	19	Ni15Co75Mn10	14.7	74.9	10.4
8	Ni46Co10Mn44	45.3	9.6	45.1	20	Ni30Co60Mn10	29.9	59.9	10.2
11	Ni15Co55Mn30	14.8	54.9	30.3	21	Ni50Co40Mn10	49.0	40.8	10.2
12	Ni30Co40Mn30	29.4	40.3	30.3	22	Ni70Co20Mn10	69.2	20.4	10.4

Table 4. Lattice parameter of FCC alloys measured in this work

Alloy composition	Lattice Parameter(Å)
$Ni_{20}Co_{10}Mn_{70}$	3.6791
$Ni_{7}Co_{30}Mn_{63}$	3.6530
$Ni_{7}Co_{40}Mn_{53}$	3.6401
$Ni_{46}Co_{10}Mn_{44}$	3.6388
$Ni_{36}Co_{20}Mn_{44}$	3.6390
$Ni_{26}Co_{30}Mn_{44}$	3.6394
$Ni_{17}Co_{40}Mn_{43}$	3.6398
$Ni_{50}Co_{20}Mn_{30}$	3.6072
$Ni_{30}Co_{40}Mn_{30}$	3.6028
$Ni_{15}Co_{55}Mn_{30}$	3.5885

Table 5. Summary of hardness tests in Co-Mn-Ni samples annealed at 1000°C for 24h.

Average is for 7 measurements and STD is standard deviation

Sample	1000°C/HV		Sample	1000°C/HV	
	AVG.	STD.		AVG.	STD.
Ni7Co20Mn73	190.5	4.0	Ni30Co40Mn30	134.5	6.6
Ni20Co10Mn70	189.1	3.0	Ni50Co20Mn30	141.9	6.0
Ni7Co30Mn63	180.8	7.8	Ni70Co00Mn30	146.6	5.0
Ni7Co40Mn53	149	5.0	Ni15Co65Mn20	118.4	2.6
Ni17Co40Mn43	157	2.0	Ni30Co50Mn20	132.0	5.8
Ni26Co30Mn44	145	3.0	Ni50Co30Mn20	130.6	3.9
Ni36Co20Mn44	156.9	4.3	Ni70Co10Mn20	128.9	3.8
Ni46Co10Mn44	157.9	5.4	Ni15Co75Mn10	118.3	8.6
Ni50Co10Mn40	160.3	5.0	Ni30Co60Mn10	122.9	4.5
Ni33Co33Mn34	146.1	4.1	Ni50Co40Mn10	124.8	4.7
Ni15Co55Mn30	129.9	3.9	Ni70Co20Mn10	128.0	4.1

Table 6. The Austenite and Martensite transformation temperatures in Co-Mn-Ni alloys.

Sample	A_s(°C)	A_f(°C)	M_s(°C)	M_f(°C)	A_p(°C)	M_p(°C)	ΔT*(°C)
No.7 $Ni_{36}Co_{20}Mn_{44}$	619	647	543	497	637	523	114
No.8 $Ni_{46}Co_{10}Mn_{44}$	607	645	543	491	637	521	116
No.9 $Ni_{50}Co_{10}Mn_{40}$	635	666	593	563	660	578	82

*$\Delta T=A_p-M_p$.

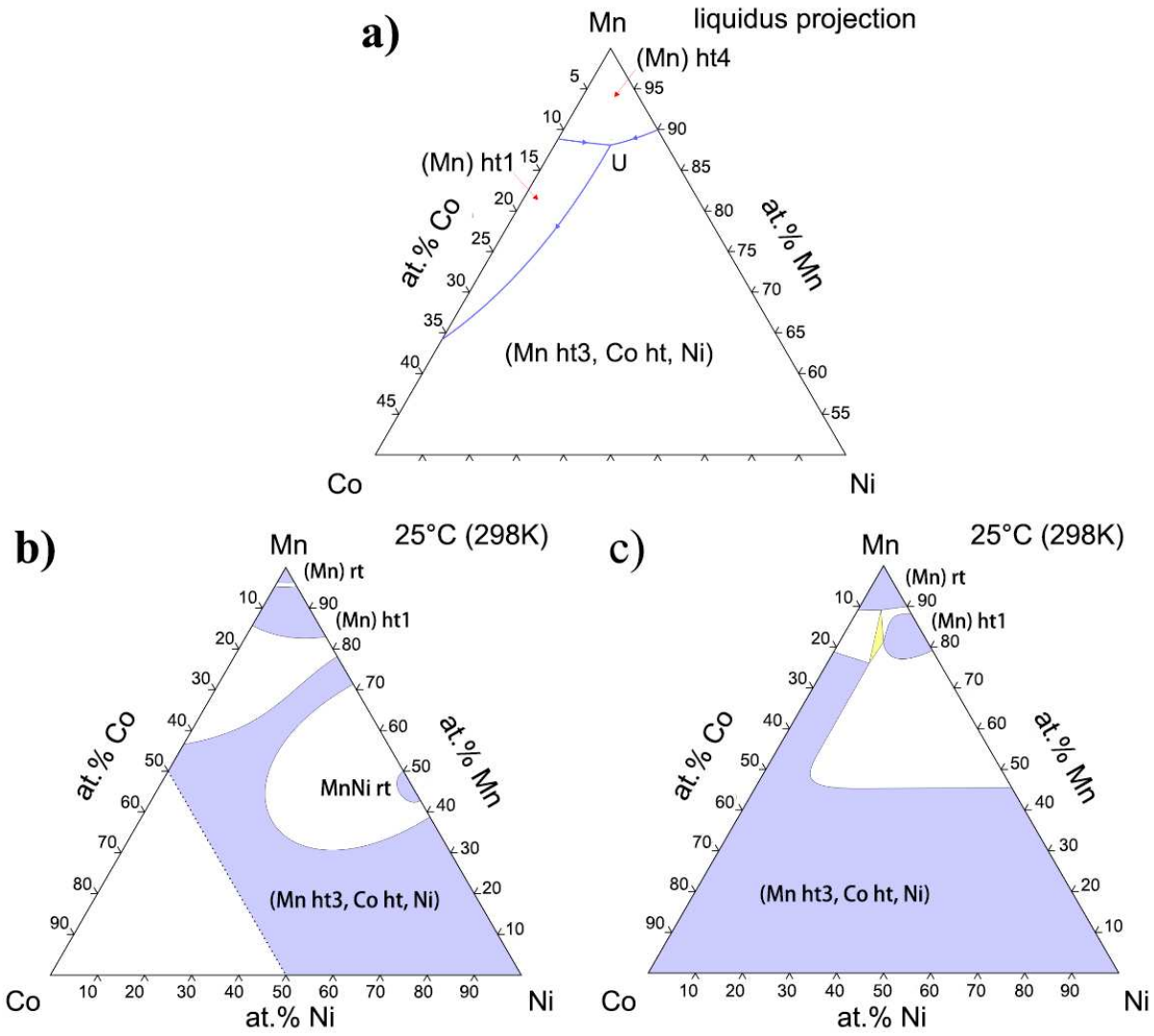
a)
liquidus projection
Mn
(Mn) ht4
(Mn) ht1
U
at.% Co
at.% Mn
(Mn ht3, Co ht, Ni)
Co
Ni
b)
25°C (298K)
Mn
(Mn) rt
(Mn) ht1
MnNi rt
(Mn ht3, Co ht, Ni)
at.% Co
at.% Mn
Co
at.% Ni
Ni
c)
25°C (298K)
Mn
(Mn) rt
(Mn) ht1
(Mn ht3, Co ht, Ni)
at.% Co
at.% Mn
Co
at.% Ni
Ni

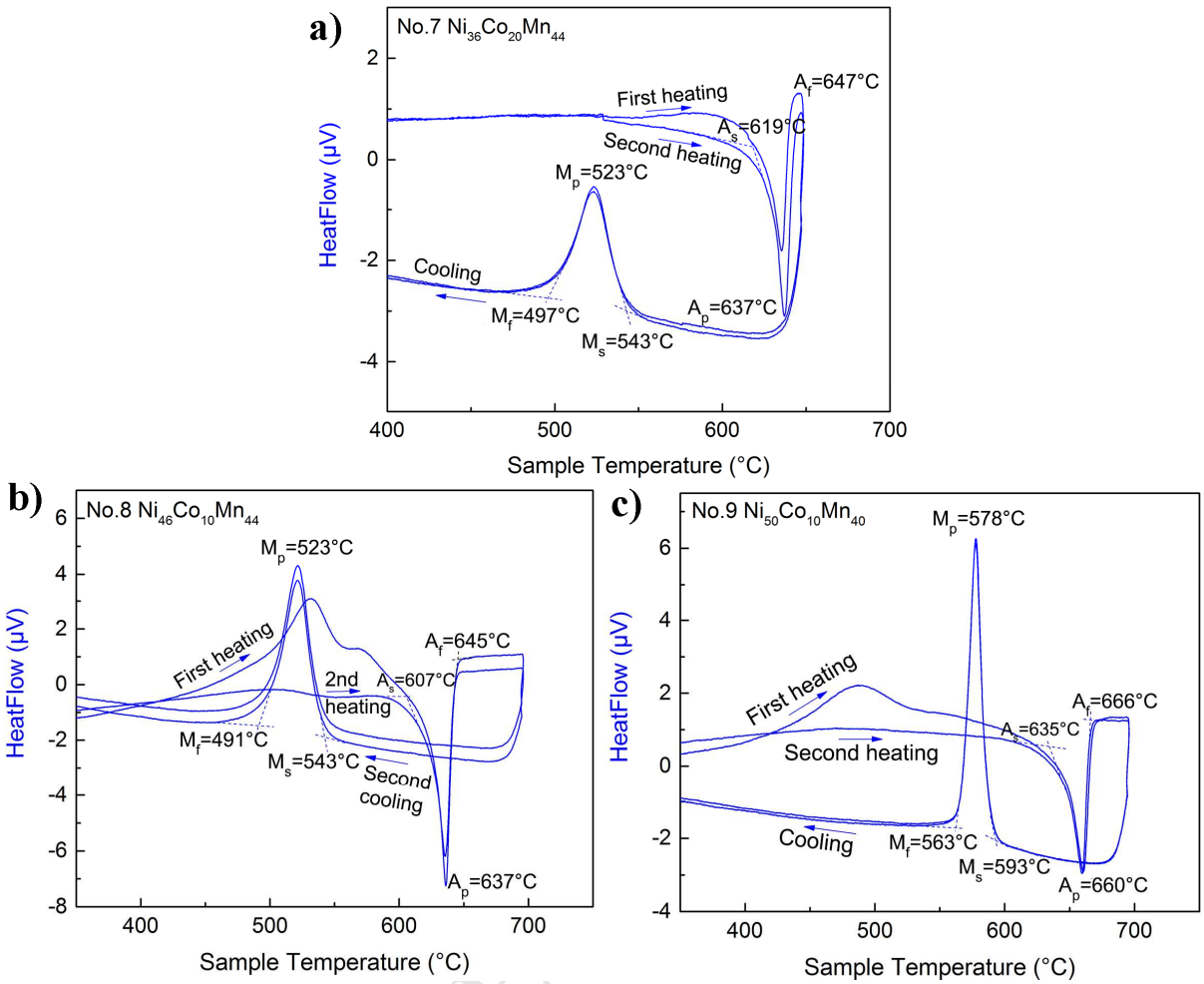
a)
No.7 Ni36Co20Mn44
First heating
Af=647°C
As=619°C
Second heating
Mp=523°C
Cooling
Mf=497°C
Ap=637°C
Ms=543°C
HeatFlow (μV)
Sample Temperature (°C)
b)
No.8 Ni46Co10Mn44
Mp=523°C
First heating
Af=645°C
2nd heating
As=607°C
Mf=491°C
Ms=543°C
Second cooling
Ap=637°C
HeatFlow (μV)
Sample Temperature (°C)
c)
No.9 Ni50Co10Mn40
Mp=578°C
First heating
Af=666°C
As=635°C
Second heating
Cooling
Mf=563°C
Ms=593°C
Ap=660°C
HeatFlow (μV)
Sample Temperature (°C)

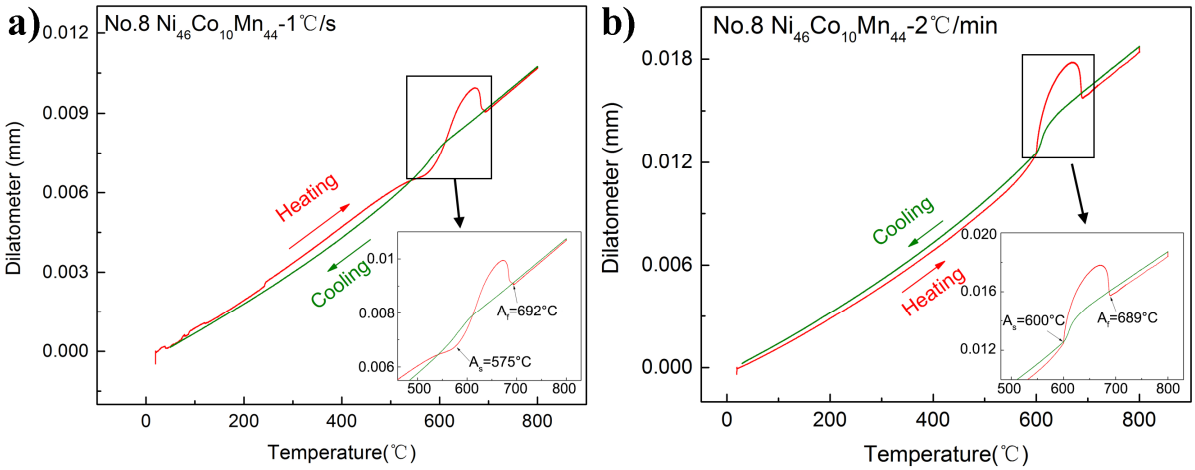

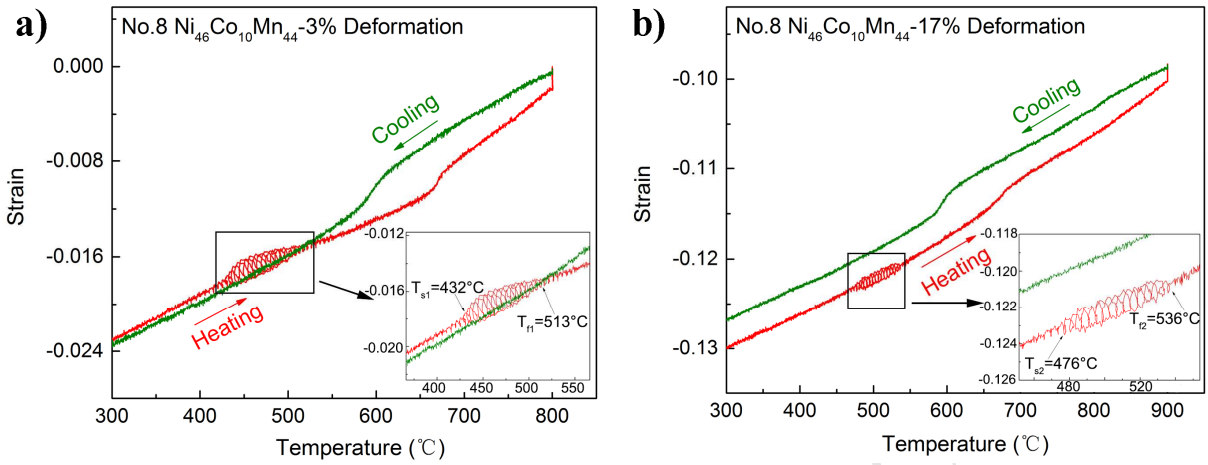

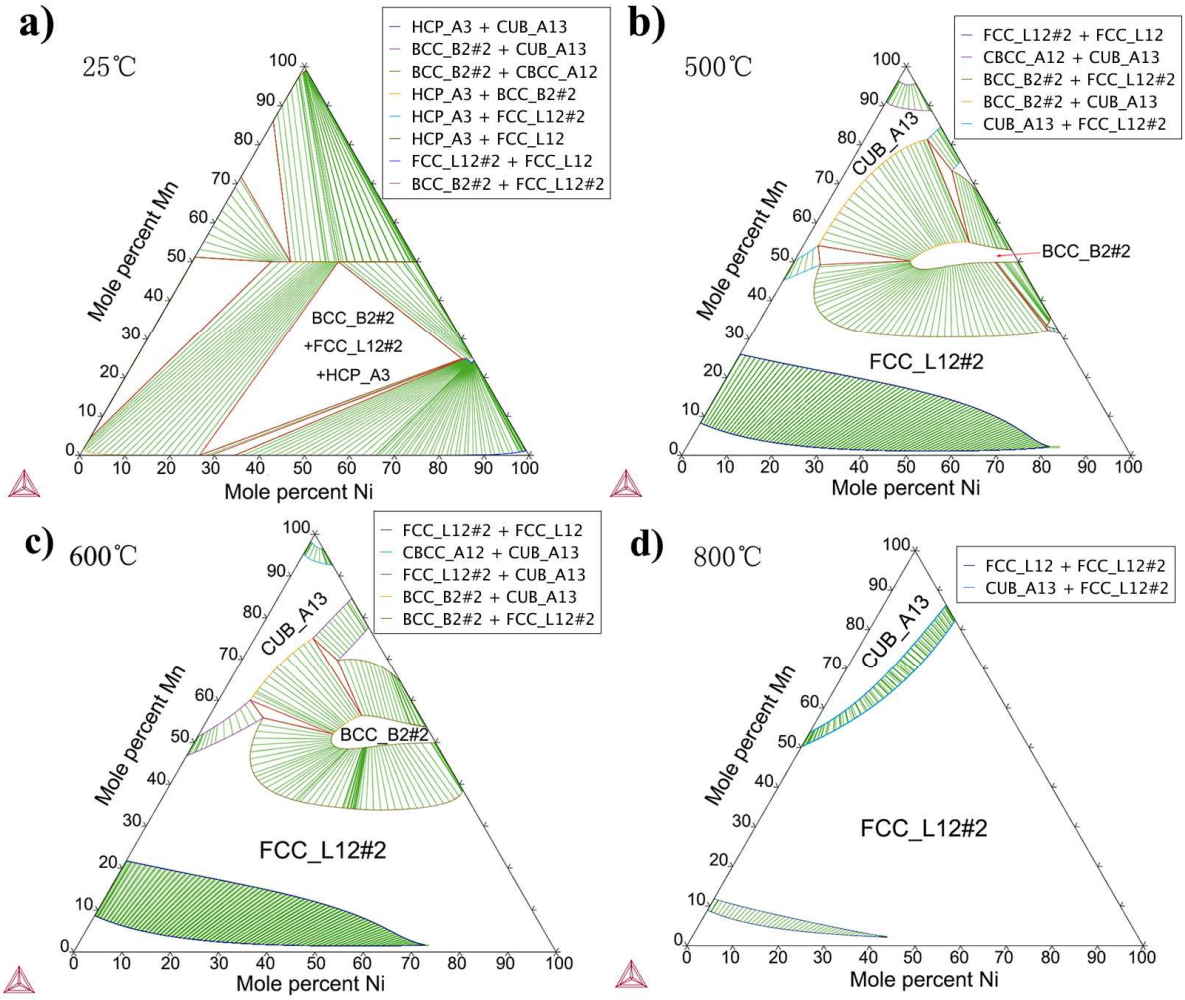
a)
25℃
HCP_A3 + CUB_A13
BCC_B2#2 + CUB_A13
BCC_B2#2 + CBCC_A12
HCP_A3 + BCC_B2#2
HCP_A3 + FCC_L12#2
HCP_A3 + FCC_L12
FCC_L12#2 + FCC_L12
BCC_B2#2 + FCC_L12#2
BCC_B2#2
+FCC_L12#2
+HCP_A3
Mole percent Mn
Mole percent Ni
b)
500℃
FCC_L12#2 + FCC_L12
CBCC_A12 + CUB_A13
BCC_B2#2 + FCC_L12#2
BCC_B2#2 + CUB_A13
CUB_A13 + FCC_L12#2
CUB_A13
BCC_B2#2
FCC_L12#2
Mole percent Mn
Mole percent Ni
c)
600℃
FCC_L12#2 + FCC_L12
CBCC_A12 + CUB_A13
FCC_L12#2 + CUB_A13
BCC_B2#2 + CUB_A13
BCC_B2#2 + FCC_L12#2
CUB_A13
BCC_B2#2
FCC_L12#2
Mole percent Mn
Mole percent Ni
d)
800℃
FCC_L12 + FCC_L12#2
CUB_A13 + FCC_L12#2
CUB_A13
FCC_L12#2
Mole percent Mn
Mole percent Ni

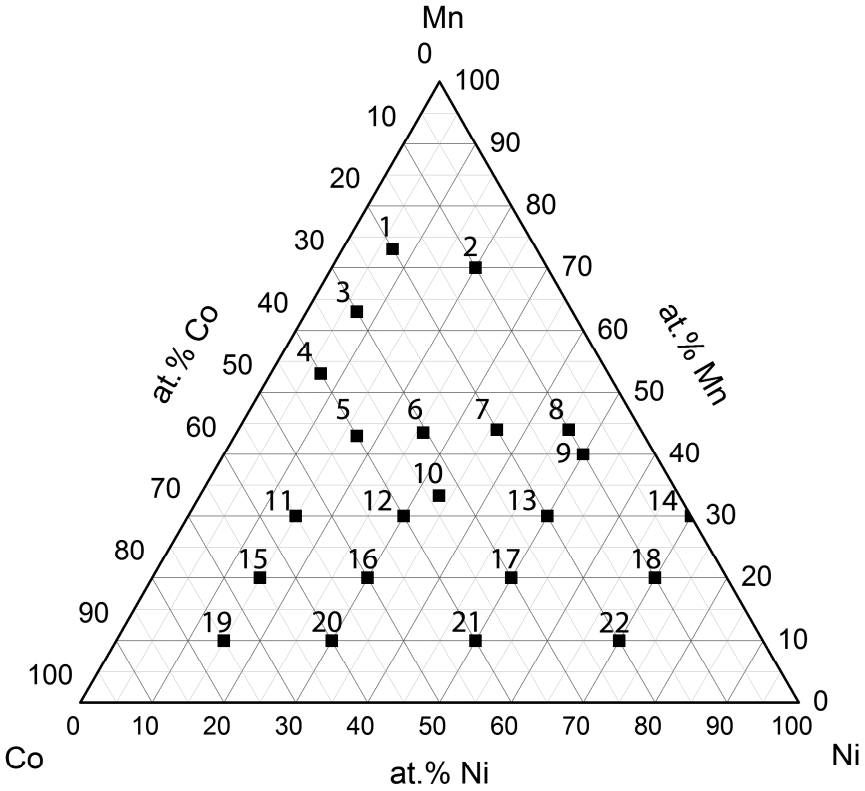

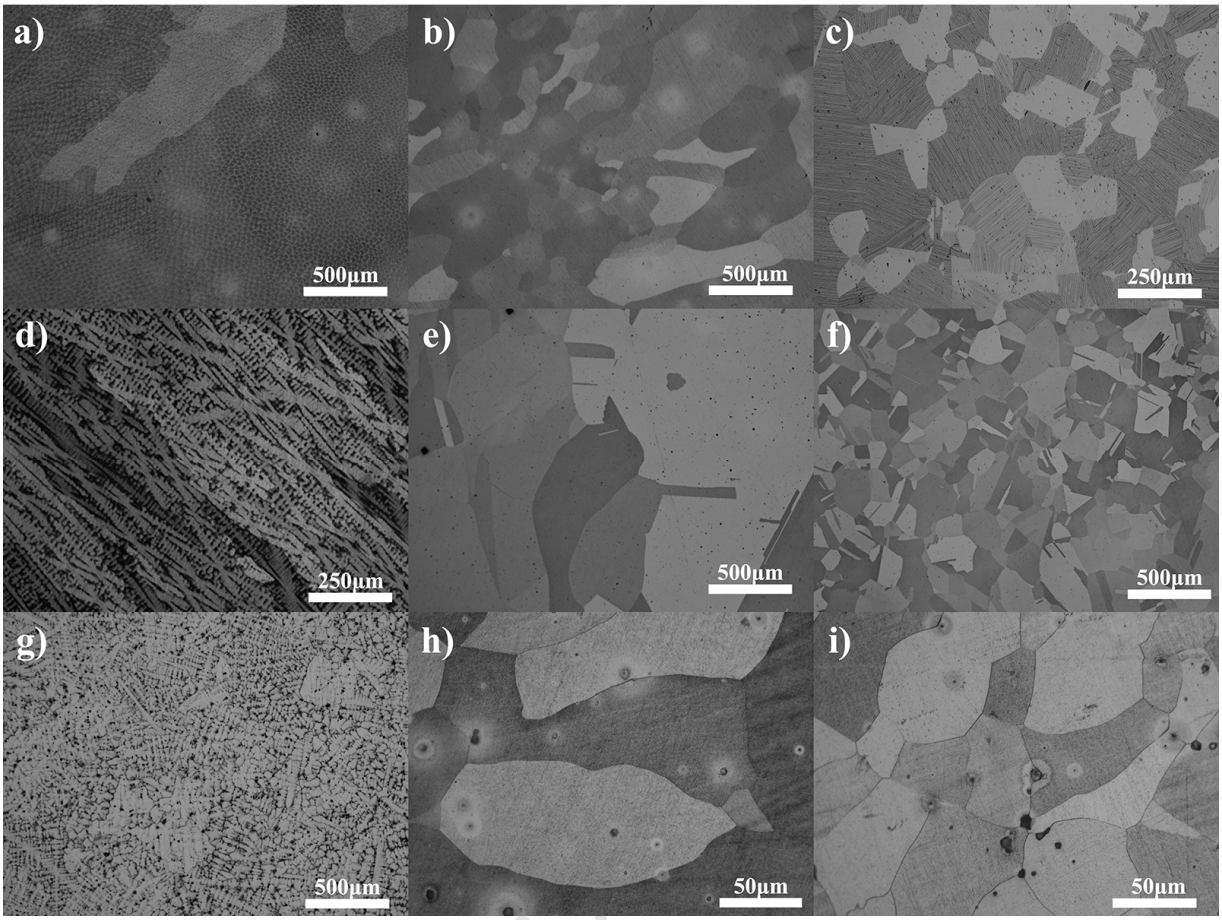
a)
500μm
b)
500μm
c)
250μm
d)
250μm
e)
500μm
f)
500μm
g)
500μm
h)
50μm
i)
50μm

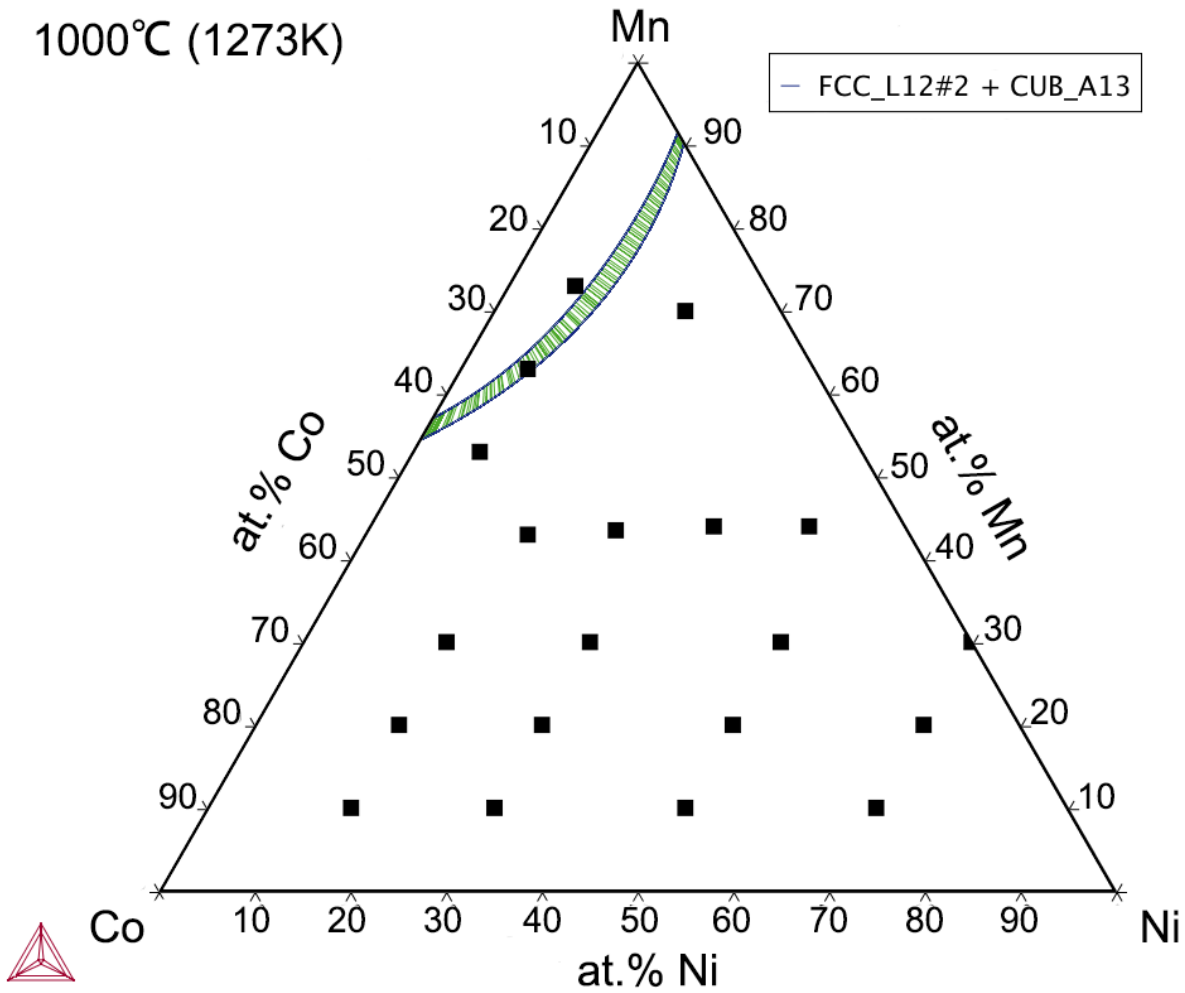

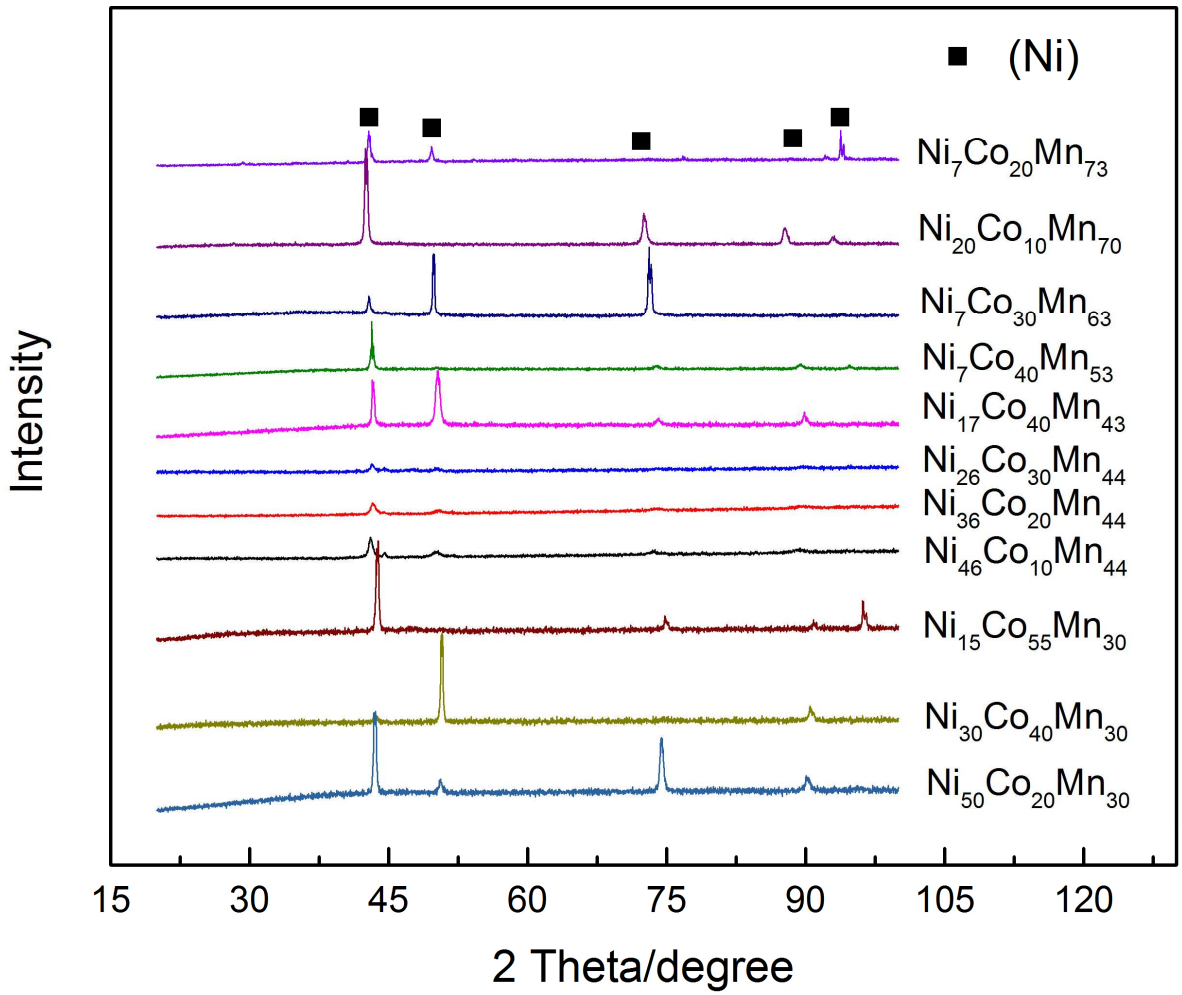

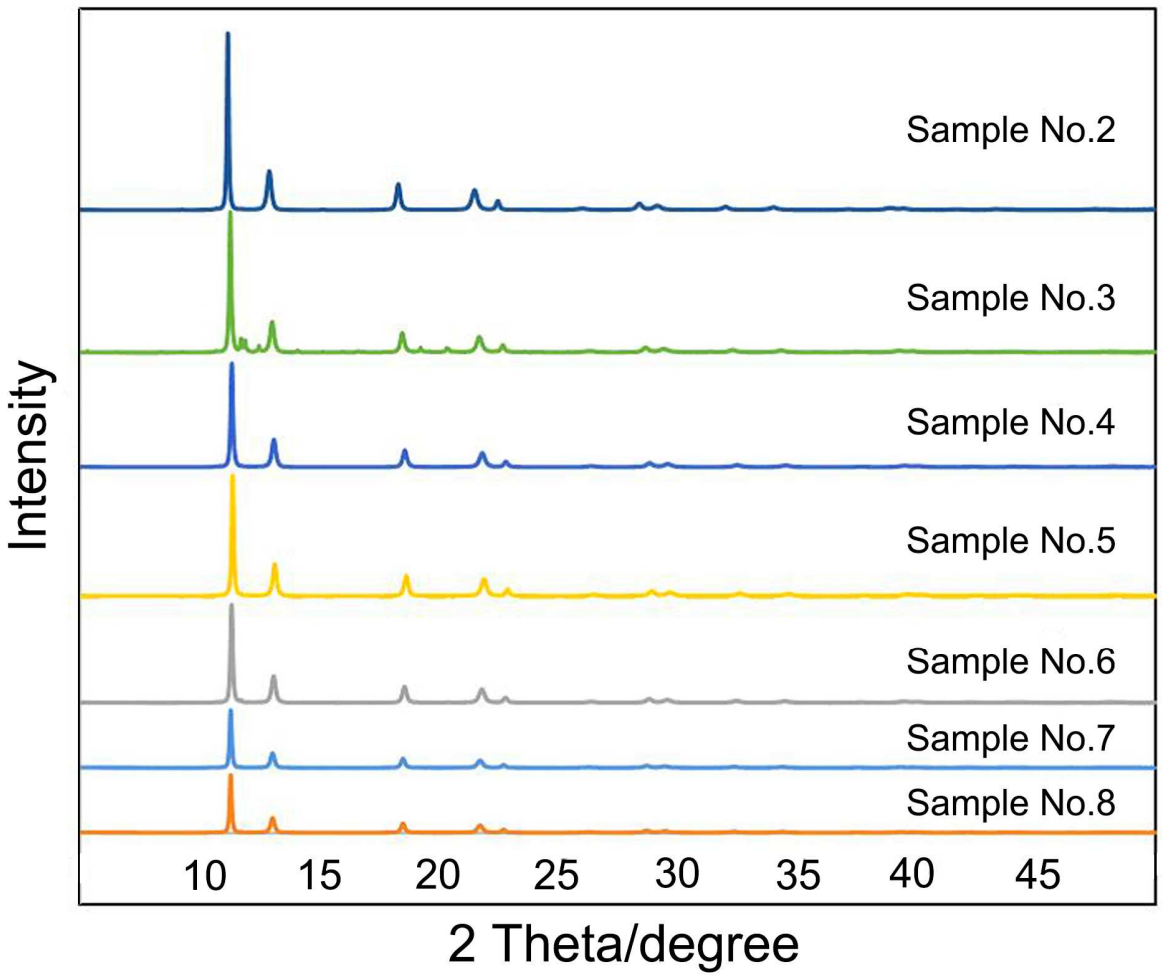
Intensity
Sample No.2
Sample No.3
Sample No.4
Sample No.5
Sample No.6
Sample No.7
Sample No.8
10
15
20
25
30
35
40
45
2 Theta/degree

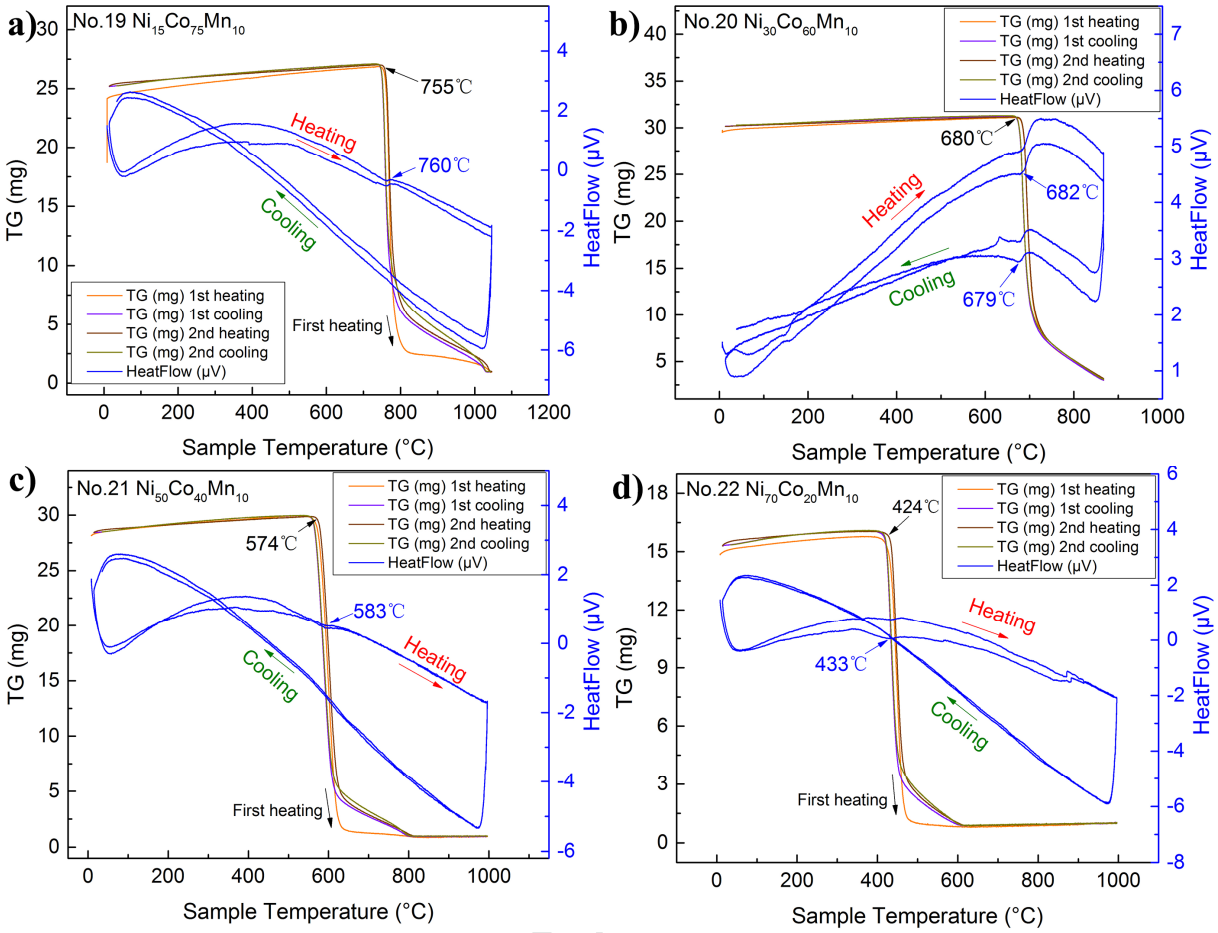

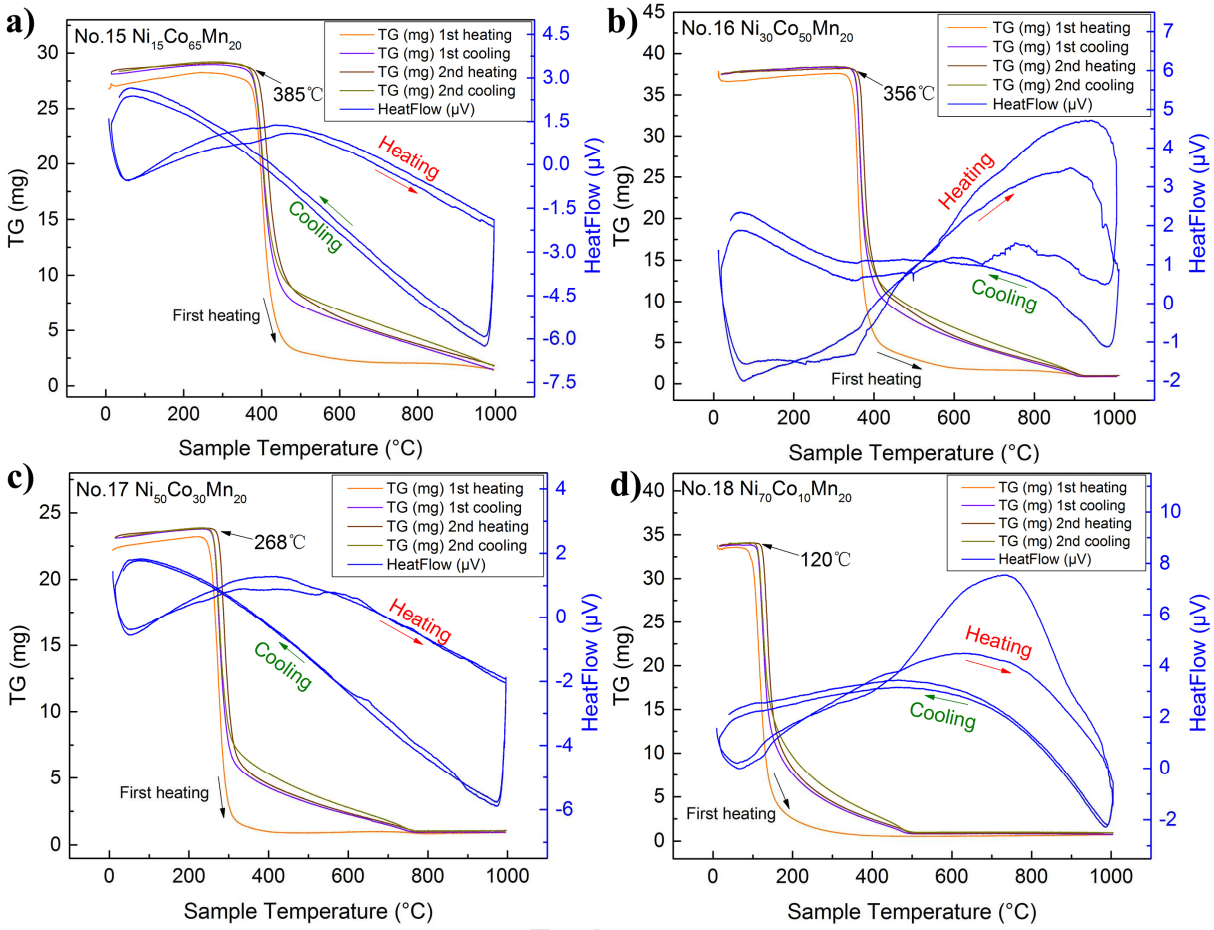
a)
No.15 Ni15Co65Mn20
TG (mg) 1st heating
TG (mg) 1st cooling
TG (mg) 2nd heating
TG (mg) 2nd cooling
HeatFlow (μV)
385℃
Heating
Cooling
First heating
TG (mg)
HeatFlow (μV)
Sample Temperature (°C)
b)
No.16 Ni30Co50Mn20
356℃
c)
No.17 Ni50Co30Mn20
268℃
d)
No.18 Ni70Co10Mn20
120℃

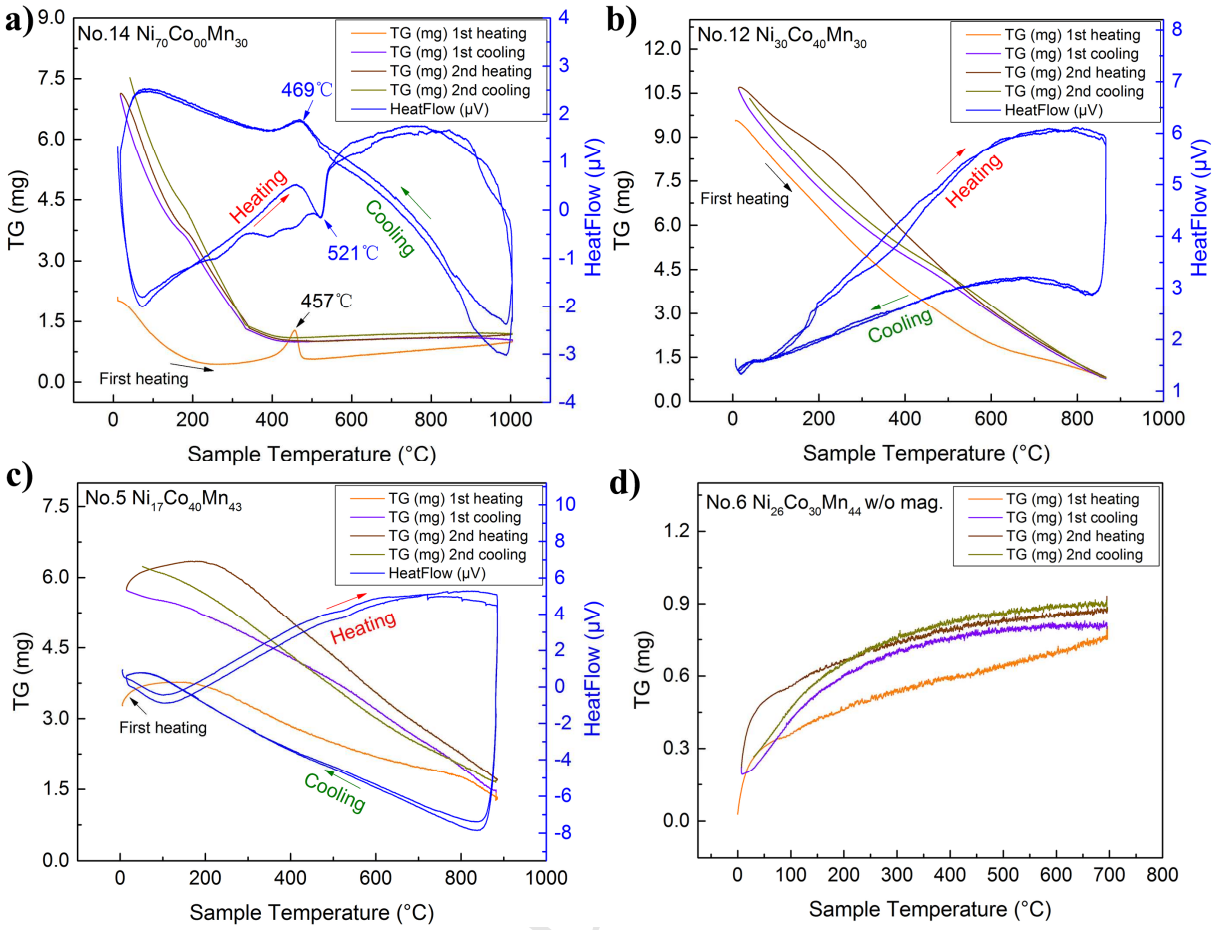

Highlights

- A partial isothermal section of the Co-Mn-Ni system at 1000°C was established
- The Curie temperature was determined using a combined magnetic TG and DSC method
- Austenitic and Martensitic transition temperatures were determined from DSC curves
- The FCC-BCC phase transformation is a thermoelastic transformation
- The shape memory effect was not observed in the Co-Mn-Ni alloys